Sahoo and Mishra
Journal of Engineering and Applied Science (2024) 71:117
https://doi.org/10.1186/s44147-024-00447-1

Journal of Engineering and Applied Science

RESEARCH Open Access

Experimental characteristic evaluation of micro hole EDM drilling of $Ni_{51.58}Ti_{48.34}$ alloy with copper electrode and response optimization using GRG assisted with GA

Amiya Kumar Sahoo[1] and Dhananjay R. Mishra[2*]

*Correspondence:
dm30680@gmail.com

[1] Department of Mechanical Engineering, Jaypee University of Engineering and Technology, A-B Road, Raghogarh, Guna 473226, Madhya Pradesh, India
[2] Department of Mechanical Engineering, Centre of Excellence for Renewable Energy, Jaypee University of Engineering and Technology, A-B Road, Raghogarh, Guna 473226, Madhya Pradesh, India

Abstract

Nitinol, a biocompatible material, is gradually becoming famous for its superelasticity, shape memory and corrosion resistance behaviours. However, the lower machinability due to the strain-hardening effect and lower thermal conductivity is contrary to its adventitious properties. Therefore, EDM is a preferable machining process for materials like Nitinol. EDM, thermal processing, raises the concern of processing Nitinol with minimal variation of its well-known properties and economical machining process. Therefore, this article deals with multi-objective optimization through GRG-assisted GA of μ-EDM drilling of $Ni_{51.58}Ti_{48.34}$ alloy using a copper electrode and distilled water. It was found that discharge current and servo voltage significantly influence the responses. The GA, with the assistance of GRG, optimized the multiple responses (viz. MRR, TWR and DoT) and yielded a discharge current of 12 A, gap voltage of 40 V, discharge time of 2 μs, charging time of 9 μs and flushing pressure of 50 kg/cm^2. The confirmatory experiment yielded MRR of 0.0036 g/min, TWR of 0.0038 g/min and DoT of 0.0089 radians. There were variations of the predicted and experimentally validated responses by − 2.78, 26.32 and 35.96% for MRR, TWR and DoT, respectively.

Keywords: EDM drilling, Copper electrode, Dielectric fluid, Nitinol, Grey relational grade, Genetic algorithm, Stochastic optimization

Introduction

Nitinol is a biocompatible material suited for various devices in medical uses [1]. It is well recognized for its superelasticity behaviour and smartness properties, like shape memory, which finds applications such as actuators and fasteners [2]. It is an almost equiatomic composition of nickel and titanium and is an intermetallic compound. However, Nitinol is hard to cut because of its high ductility, low thermal conductivity and strain-hardening effect [3]. EDM is an unconventional technique dealing with material removal by the sparks generated in the electrode-work gap. EDM can remove material from electrically conductive materials, including hard-to-cut ones like Nitinol [4].

Various researchers investigated EDM operations on exotic materials to evaluate their performance and characterize them [5–9].

Chakala et al. [10] studied the optimization of WEDM for Nitinol through RSM and desirability approach and found that uneven surfaces due to craters and recast layers directly vary with current and exposure time.

Kim et al. [11] studied and optimized electropolishing of Nitinol stent and found improved corrosion resistance characteristics at lower roughness. Lee and Shin [12] experimented with laser-direct deposition of Nitinol and stated that precipitates are incoherent with the matrix after the ageing heat treatment that raises the transformation temperature. Li et al. [13] underwent a biocompatibility study of Nitinol through the micro- or nanostructures created using a nanosecond laser, and the oxide films of titanium and nickel were produced to provide better cell growth on the implant. Chaudhari et al. [14] analysed the WEDMed Nitinol surface and found that surface roughness rises with discharge energy. Lojen et al. [15] tried continuous casting of Nitinol and verified the presence of various compounds like Ti_2Ni, TiNi and $TiNi_3$ under different casting conditions. Datta et al. [16] optimized the process of LBW of Nitinol through various metaheuristic practices and found satisfactory predicted results validated by experimentation for minimum variation of micro-hardness of the weld. Ikeuchi et al. [17] investigated EDM characteristics for LaB_6 work material and found that material fracturing leads to material removal along with common causes such as melting and evaporation. Ming et al. [18] compared the behaviour of magnetic-assisted EDM on ferromagnetic and diamagnetic materials. They concluded that the MRR rises for both, and the higher rise of MRR was seen for ferromagnetic work material. Ilani and Khoshnevisan [19] investigated the PM-EDM on titanium grade-5 alloy using an FDMed copper electrode and found enhancements in MRR, TWR and surface finish with the most remarkable improvement in the surface quality. Paswan et al. [20] investigated EDM operations on MMC using steam as dielectric instead of kerosine in the die-sinking method and found improvement concerning the recast layer and yield as a sustainable process. Baran and Polanski [21] verified the microstructure of Nitinol through laser processing of net shape products and stated that at low scanning speed, it yielded lower superelasticity and shape memory behaviour, whereas the axial grains formed at higher scanning speed. Pelton et al. [22] optimized the process and the properties of Nitinol and stated that the shape memory property could be retained by accurately fixing the transformation temperature through a selective ageing heat-treatment process. Roy and Mandal [23] studied WEDM through surface integrity of Nitinol and concluded that the crack density rises with the rise in the flow of the dielectric that quenches the material efficiently, and recast layers on it confirmed that the higher flow was unable to flush the removed material properly. Lee and Shin [24] completed electrochemical polishing of Nitinol for the machinability study and stated that at a higher current and lower interelectrode gap, the surface finish is better. Kowalczyk and Nizankowski [25] experimented with the turning of Nitinol materials and studied their machinability through a weighted radar diagram and found that the machinability of β-Nitinol is better than α-Nitinol.

Shiek et al. [26] experimented with the PMEDM process to enhance MRR for Ti alloy and stated that the powder concentration up to 4 g/positively impacts MRR. Sharma et al. [27] reported EDM operation on stainless steel and stated that copper electrodes

were better than brass electrodes regarding hole circularity. Quarto et al. [28] reported optimization of the micro-EDM using PSO and ANN and indicated that the two-step method provides operator flexibility to select the parameter required to optimize the process for the best solution. Abhilash and Chakradhar [29] completed multi-attribute optimization of WEDM of Inconel 718 through GRA-TOPSIS and emphasized that the entropy-weighted TOPSIS provides a better process concerning the TOPSIS alone. Naik and Sathisha [30] optimized micro-channelling using the EDM process on silicon wafer and stated that PSO gave the required convergence for the machining conditions using sodium hydroxide and potassium hydroxide as the mixed dielectric fluid. Ram et al. [31] experimented with WEDM operation on MMC based on Al6351 and stated that discharge time and current were the best factors controlling kerf width and surface roughness concerning wire feed. Pandey et al. [32] conducted a vibration-assisted EAM process on aluminium and boron carbide MMC and stated that a single objective optimization process based on the AI approach significantly improved MRR. Sisodiya et al. [33] studied Maglev EDM on pure titanium and found improvements compared to the traditional EDM procedure. Kiran et al. [34] examined the consequences of powder material used along with the bio-dielectric fluid on the exterior of Ti-grade 5 alloy and found the dielectric and the tool materials on the substrate confirmed through EDX analysis. Baroi et al. [35] reviewed EDM's sustainability and safety issues and stated that the truly eco-friendly dielectric was water based, and selection and recirculation of dielectric with suspended powder were difficult. Ablyaz et al. [36] studied the composite electrode's impact on the steel-copper bi-metallic material and stated that micro-holes formed during the processing of the steel zone and enlarged holes formed during the processing of the other zone. Rajguru et al. [37] studied the accomplishment of a composite copper-CNT electrode on the EDM process and found that MRR and surface finish enhanced due to the modification in the tool material and possessed higher TWR. Kumar and Davim [38] investigated the impact of silicon powder mixed with the dielectric of MMC and reported that improvement in surface quality and MRR happened with a particular powder concentration. Fasina et al. [39] investigated boring on steel through comparative optimization studies and indicated that the hybrid TLBO provided better surface roughness estimation.

Muralidharan et al. [40] experimented with laser machining Nitinol and concluded a rise in micro-surface irregularity with laser energy and reduced cutting speed. Hung and Yang [41] experimented with ultrasonic-assisted electrochemical machining of Nitinol wire for micro-slots and confirmed that the slot width rises with the electrolyte concentration by the enhanced process efficiency due to the vibration assistance. Sahu et al. [42] stated the impact of an electrode on the surface finish of the EDMed Nitinol work material and found that a healthier surface finish was accomplished by the AlSiMg electrode prepared by a selective laser sintering process compared with the copper electrode. Kulkarni et al. [43] completed the optimization of multiple responses of WEDM of Nitinol and confirmed the genuinely significant process control parameter was wire feed rate, considering material removal rate and surface quality as the responses. Pradhan et al. [44] studied micromachining of Nitinol using Nd:YAG laser and concluded that the lower width deviation falls with the rise in the pulse frequency. Liu et al. [45] analysed the formation of white layer

while machining Nitinol shape memory alloy using EDM and emphasized that the nano hardness rises and the modulus of white layer falls concerning the base material. Duerig et al. [46] explored the transformation temperature of Nitinol and found that the transformation temperature can be reduced by making the material's triple point higher. Sahoo et al. [47] experimented with EDM and optimized for Nitinol through Taguchi analysis and GRG and found that the discharge time and inter-work-electrode gap voltage were the process's very influencing process parameters. Kılıç [48] utilized ANN and GIS to predict wind energy potential.

Mishra et al. [49] investigated the kerf quality of laser cutting of FRP. They optimized the process using GRA and found improvements by enhancing kerf width. Taskan et al. [50] examined the suitability of Nitinol as anode in microbial fuel cells and concluded that thick electroactive biofilm formed on the anode was suitable for achieving higher power density. Guo et al. [51] researched the machinability aspects of Nitinol. They stated that the white layer formed due to higher plastic deformation during the milling operation, whereas it is due to melting and quenching in EDM operation. Mishra et al. [52] optimized the kerf deviation of laser cutting operation using GRA and indicated improvement in cut quality with stand-off distance as the significant parameter. Paszkowicz [53] studied the application of genetic algorithm (GA) in the related fields of material science and stated that GA is an efficient tool to optimize problems with a higher number of process control parameters having several local maxima or minima. Bhoskar et al. [54] reviewed the utilization of GA in mechanical engineering and concluded that GA, a stochastic approach, is a nondeterministic method for searching for the optimum value through nature-inspired evolution and natural selection. Reddy et al. [55] utilized GA to optimize laser machining operation on Hastelloy C-276 and stated that the pulsated laser frequency has a more momentous impact on the surface unevenness, whereas the scanning speed of the laser influences the milling depth more than the other parameters. Kilickap et al. [56] used GA to optimize drilling operation on AISI 1045 steel for surface roughness by a TiN-coated HSS drill through the response surface methodology. Gautam and Mishra [57] evaluated the geometric features of laser cutting of KBFRP hybrid composite using GRGA and found 31.23% overall improvements in the cut quality characteristics. Guo et al. [58] purported a new deformation method prediction by changing early residual stress based on regression analysis of support vector and GA and confirmed that the residual stress lowered to 15.45% from 31.1%.

The biocompatible, superelastic, and shape memory material, i.e. Nitinol, needs to be machined using advanced machining processes like EDM for better product accuracy. The heat of the spark in the EDM operation is responsible for material removal, which has consequences on the Nitinol product's behaviour. Hence, the EDM drilling of Nitinol needs an optimized process to enhance the economy and the accuracy of the processed product. The optimization also considers the required properties essential for using Nitinol material. Therefore, micro EDM drilling on Nitinol has been reported in this manuscript, including its characterization and optimization using a genetic algorithm assisted with the grey relational grade for tri-response analysis considering material removal rate, tool wear rate and degree of hole taper as the responses.

Methods

This experimental work was completed using a three-phase methodology, as shown in Fig. 1. The first phase consists of experimental trial runs to select the levels of process parameters. In the next step, the Box-Behnken design (BBD) was used for the experimental design, in which five process control parameters with their three different levels were selected along with six replications of the centre point, a total of 46 experiments. In the next step, the experimental work was carried out concerning the BBD DOE, and the responses were evaluated for their mathematical modelling to check their suitability. The grey relational analysis (GRA) was completed in the second phase. The second phase includes normalization, calculation of grey relational grades (GRG) and mathematical modelling of GRG. A genetic algorithm (GA) was implemented in the last phase to optimize the response.

The Sparkonix EDM machine was used to carry out the experimental work. The actual photograph of the machine is demonstrated in Fig. 2. There are five process control parameters such as discharge current ranging from 1 to 25 A with steps of 1 A, servo-controlled gap voltage ranging from 10 to 100 V with steps of 10 V, the charging and discharging times ranging from 1 to 10 µs with steps of 1 µs and discharge pressure of dielectric fluid up to 100 kg/cm^2.

The EDM drilling can be easily comprehended through the schematic shown in Fig. 3. The schematic shows all the essential components of EDM drilling, including the sparking between the tool-work gap, removal work material, electrode wear, recast layer, hole tapper, and dielectric flushing.

This experimental work used Nitinol with a substance composition of 51.58% Ni and 48.34% Ti and 6-mm thickness. The copper tubular electrodes used for drilling were 0.5 mm in diameter. The BBD design used five process parameters with three levels

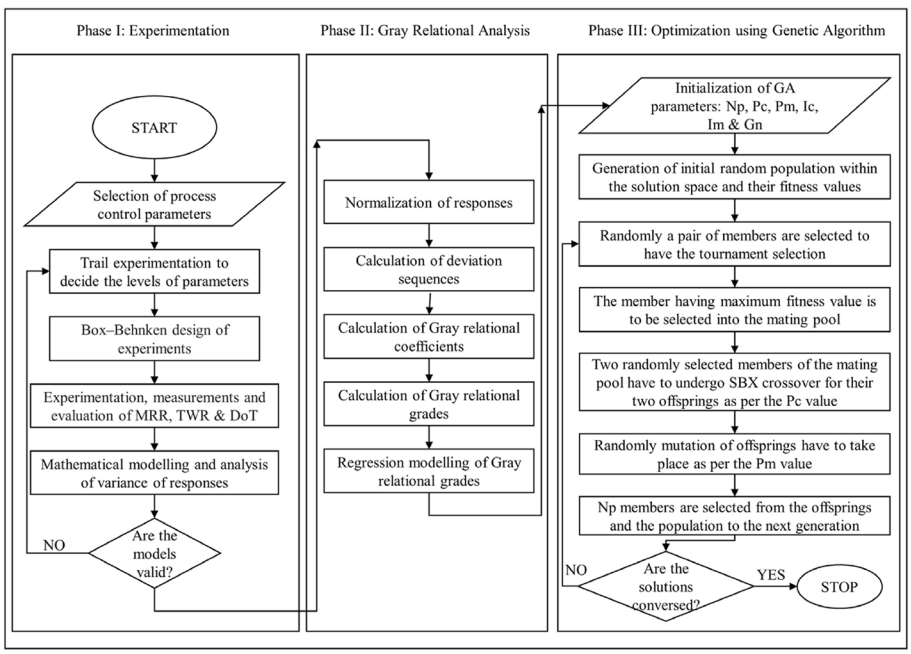

Fig. 1 Graphical representation of the work

Fig. 2 Photograph of Sparkonix EDM drilling machine

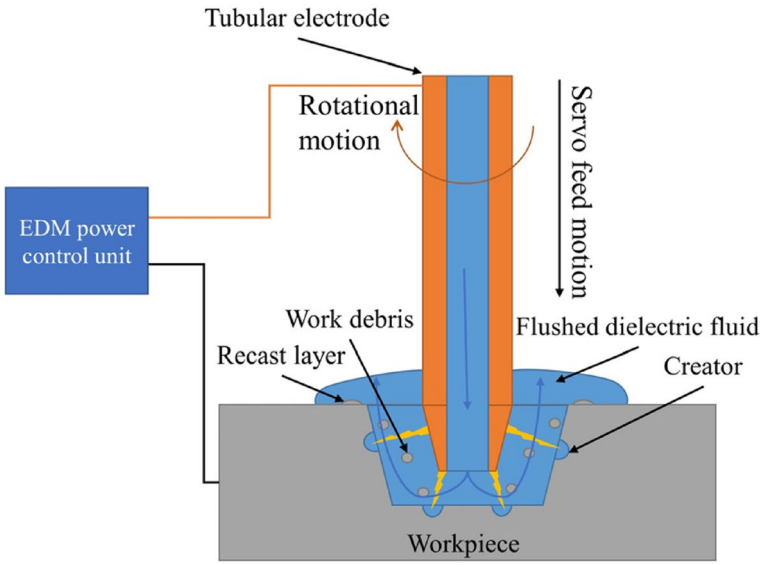

Fig. 3 Representation of EDM drilling operation

due to its non-linear sensitivity of the responses considered. The BBD yielded 46 sets of experiments, including 6 centre-point repetitions. The process parameters and their levels considered in the experimental work are given in Table 1.

Table 1 Process parameters and their levels used for the experimental work

Sl	Parameter	Unit	Level 1	Level 2	Level 3
1	Discharge current (I)	A	12	17	22
2	Gap voltage (V)	V	40	50	60
3	Discharging times (T_{ON})	µs	2	4	6
4	Charging times (T_{OFF})	µs	5	7	9
5	Dielectric pressure (DP)	Kg/cm^2	50	75	100

The weight measurements before and after the EDM drilling were completed during the experimentation for the electrode and the workpiece. A weighing machine with a precision of 0.001 g was used. Also, the action times were recorded with a precision of 0.001 s to estimate the material removal rate (MRR) and tool wear rate (TWR) as two responses. Furthermore, the third response degree of hole taper (DoT) was evaluated by measuring both side hole diameters with a precision of 0.01 mm. The diameters were evaluated as the average of six measurements at different orientations of the drilled holes. The responses considered are MRR, TWR and DoT, calculated using Eqs. 1, 2 and 3 and tabulated in Table 2. Figure 4 shows the photographs of the workpiece on both sides, indicating the corresponding experiment numbers.

$$MMR = \frac{weight\ of\ workpiece\ (before - after)\ drilling}{drilling\ time} \tag{1}$$

$$TWR = \frac{weight\ of\ electrode\ (before - after)\ drilling}{drilling\ time} \tag{2}$$

$$DoT = \tan^{-1}\left[\frac{average(top - bottom)\ diameter\ of\ hole}{2 \times\ thickness\ of\ the\ workpiece}\right] \tag{3}$$

The mathematical analysis of the results had been completed before moving to the optimization process using GA. In this work, three responses were recorded as MRR, TWR and DoT, from which MRR needs to be maximized and TWR and DoT need to be minimized. In addition, the different goals for each response needed to be unified to have one optimisation goal. Therefore, grey relational analysis was considered the unified mathematical mechanism [29] where the responses were normalized per their requirements. Hence, Eqs. 4 and 5 were used to maximize MRR and minimize TWR and DoT, respectively.

$$X_{Ni} = \frac{X_{in} - X_{\min.}}{X_{\max.} - X_{\min.}} \tag{4}$$

$$X_{Ni} = \frac{X_{\max.} - X_{in}}{X_{\max.} - X_{\min.}} \tag{5}$$

where X_{Ni}, X_{in}, X_{max} and X_{min} are the normalized i^{th} response, i^{th} response, top value of responses and bottom value of responses, respectively.

Table 2 Experiments as per BBD with responses (MRR, TWR & DoT)

Sl	I (A)	V (V)	T_{ON} (μs)	T_{OFF} (μs)	DP (kg/cm^2)	MRR (g/min)	TWR (g/min)	DoT (rad)
1	22	50	4	5	75	0.0042	0.0280	0.0085
2	17	60	6	7	75	0.0036	0.0350	0.0096
3	17	40	2	7	75	0.0089	0.0117	0.0004
4	17	50	4	7	75	0.0061	0.0196	0.0081
5	17	50	2	7	50	0.0059	0.0126	0.0028
6	17	40	4	9	75	0.0047	0.0154	0.0190
7	17	50	4	7	75	0.0078	0.0245	0.0110
8	17	60	4	7	100	0.0034	0.0363	0.0140
9	17	50	2	9	75	0.0068	0.0112	0.0103
10	17	50	6	9	75	0.0041	0.0162	0.0075
11	12	40	4	7	75	0.0061	0.0117	0.0053
12	17	50	4	7	75	0.0061	0.0221	0.0069
13	22	50	4	7	50	0.0072	0.0271	0.0125
14	22	50	2	7	75	0.0078	0.0201	0.0060
15	17	50	2	7	100	0.0068	0.0119	0.0051
16	17	40	4	7	50	0.0064	0.0229	0.0028
17	17	50	6	5	75	0.0097	0.0322	0.0082
18	12	50	2	7	75	0.0041	0.0075	0.0056
19	12	60	4	7	75	0.0026	0.0321	0.0169
20	17	50	4	5	100	0.0059	0.0278	0.0122
21	17	50	6	7	50	0.0070	0.0242	0.0069
22	17	60	2	7	75	0.0023	0.0260	0.0135
23	17	40	4	5	75	0.0095	0.0232	0.0118
24	17	50	6	7	100	0.0080	0.0290	0.0140
25	17	40	4	7	100	0.0065	0.0225	0.0074
26	17	50	4	9	50	0.0044	0.0151	0.0069
27	22	40	4	7	75	0.0059	0.0269	0.0189
28	17	60	4	9	75	0.0012	0.0344	0.0229
29	17	50	4	9	100	0.0045	0.0156	0.0175
30	22	50	4	9	75	0.0054	0.0234	0.0081
31	12	50	4	9	75	0.0044	0.0097	0.0037
32	12	50	4	7	100	0.0080	0.0138	0.0101
33	17	60	4	5	75	0.0038	0.0380	0.0121
34	17	40	6	7	75	0.0027	0.0298	0.0143
35	12	50	6	7	75	0.0068	0.0114	0.0062
36	12	50	4	7	50	0.0059	0.0150	0.0011
37	17	50	4	7	75	0.0103	0.0135	0.0232
38	22	60	4	7	75	0.0023	0.0409	0.0128
39	17	50	2	5	75	0.0087	0.0174	0.0117
40	17	50	4	5	50	0.0064	0.0262	0.0133
41	17	50	4	7	75	0.0063	0.0219	0.0178
42	12	50	4	5	75	0.0043	0.0173	0.0128
43	17	60	4	7	50	0.0021	0.0335	0.0178
44	22	50	6	7	75	0.0049	0.0330	0.0133
45	22	50	4	7	100	0.0052	0.0302	0.0114
46	17	50	4	7	75	0.0061	0.0195	0.0175

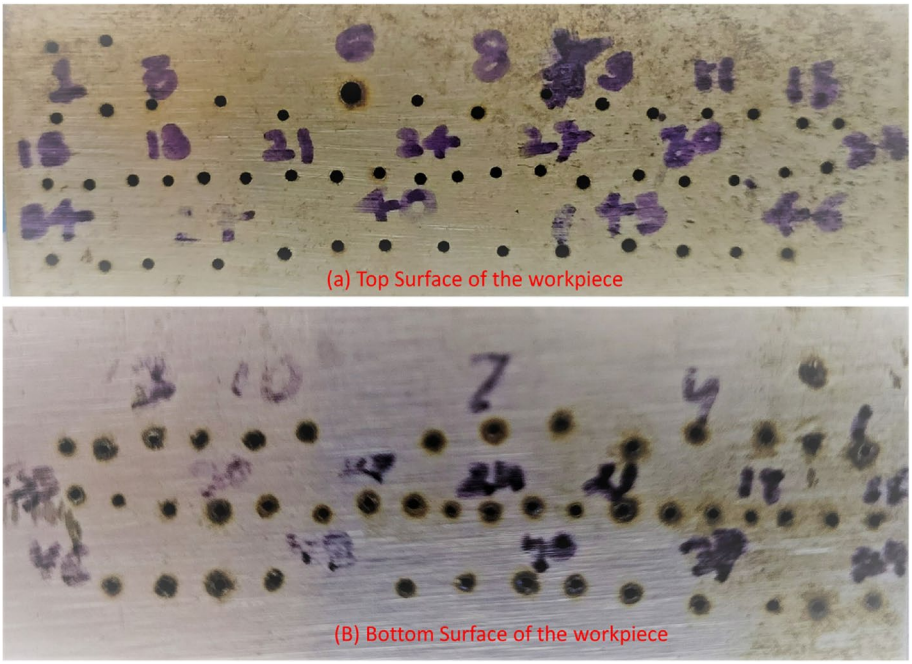

Fig. 4 Images of both sides of EDM drilled workpiece

The deviation sequences of each experimental set for each response were calculated as the deviation of the maximum and the corresponding values. After that, the grey relational coefficients (GRCs) for each response were calculated using Eq. 6. Finally, the unified responses as the grey relational grades (GRGs) were estimated using Eq. 7. The normalized responses, GRCs and GRGs, are tabulated in Table 3.

$$GRC_i = \frac{\Delta X_{\text{min.}} + \zeta \times \Delta X_{\text{max.}}}{\Delta X_{in} + \zeta \times \Delta X_{\text{max.}}} \tag{6}$$

$$GRG_i = \frac{1}{n} \sum\nolimits_1^n GRC_i \tag{7}$$

where ΔX_{min}, ΔX_{max} and ΔX_{in} are the minimum, maximum and i^{th} deviation sequence of each response for each experimental set, respectively. $\zeta = 0.5$, average importance to each, generally varying between 0 and 1. The GRGs were found by averaging the GRCs of each experimental set, i.e. equal weight to each response considered.

The GRGs of the experimental sets were then used to get the mathematical modelling using multi-regression analysis as a quadratic model, as shown in Eq. 8. Furthermore, the ANOVA of GRG is shown in Table 4. The ANOVA shows that the tri-regression model is significant, with a lower p-value [59]. The ANOVA provides that the GRG model's process parameters that influence the most are servo voltage (V) and discharge current (I). The terms of the model with higher p-values have a lower influence on the GRG response. As the lack of fit is insignificant, the model does not overfit. It can be well understood through the fit statistics, which provide a difference of less than 0.2 between the adjusted R^2 and the predicted R^2 values, and the signal-to-noise ratio is greater than the 4 required.

Table 3 Normalized values, GRCs and GRGs of each experiment

Sl	Normalized responses			Grey relational coefficients			GRG
	MRR	TWR	DoT	MRR	TWR	DoT	
1	0.3313	0.3879	0.6463	0.4278	0.4496	0.5857	0.4877
2	0.2636	0.1780	0.5975	0.4044	0.3782	0.5540	0.4455
3	0.8484	0.8760	1.0000	0.7673	0.8013	1.0000	0.8562
4	0.5370	0.6395	0.6646	0.5192	0.5810	0.5985	0.5663
5	0.5165	0.8470	0.8963	0.5084	0.7657	0.8283	0.7008
6	0.3845	0.7635	0.1829	0.4482	0.6789	0.3796	0.5022
7	0.7343	0.4913	0.5365	0.6530	0.4957	0.5190	0.5559
8	0.2463	0.1378	0.4024	0.3988	0.3671	0.4555	0.4071
9	0.6166	0.8915	0.5670	0.5660	0.8216	0.5359	0.6412
10	0.3165	0.7393	0.6890	0.4225	0.6573	0.6165	0.5654
11	0.5397	0.8745	0.7865	0.5207	0.7994	0.7008	0.6736
12	0.5426	0.5641	0.7134	0.5223	0.5343	0.6356	0.5640
13	0.6623	0.4145	0.4694	0.5968	0.4606	0.4852	0.5142
14	0.7344	0.6235	0.7561	0.6531	0.5704	0.6721	0.6319
15	0.6135	0.8681	0.7926	0.5640	0.7913	0.7069	0.6874
16	0.5750	0.5408	0.8963	0.5405	0.5213	0.8283	0.6300
17	0.9341	0.2616	0.6585	0.8835	0.4037	0.5942	0.6271
18	0.3262	1.0000	0.7744	0.4260	1.0000	0.6890	0.7050
19	0.1584	0.2645	0.2743	0.3727	0.4047	0.4079	0.3951
20	0.5215	0.3924	0.4816	0.5110	0.4514	0.4910	0.4845
21	0.6395	0.4994	0.7134	0.5810	0.4997	0.6356	0.5721
22	0.1252	0.4460	0.4268	0.3637	0.4744	0.4659	0.4347
23	0.9166	0.5304	0.4999	0.8570	0.5157	0.5000	0.6242
24	0.7515	0.3568	0.4024	0.6680	0.4374	0.4555	0.5203
25	0.5859	0.5516	0.6951	0.5470	0.5272	0.6212	0.5651
26	0.3549	0.7731	0.7134	0.4366	0.6878	0.6356	0.5867
27	0.5226	0.4207	0.1890	0.5116	0.4633	0.3814	0.4521
28	0.0000	0.1949	0.0122	0.3333	0.3831	0.3361	0.3508
29	0.3666	0.7577	0.2499	0.4411	0.6736	0.4000	0.5049
30	0.4619	0.5245	0.6646	0.4816	0.5126	0.5985	0.5309
31	0.3506	0.9361	0.8536	0.4350	0.8867	0.7736	0.6984
32	0.7481	0.8121	0.5731	0.6650	0.7268	0.5394	0.6437
33	0.2835	0.0878	0.4877	0.4110	0.3541	0.4939	0.4197
34	0.1616	0.3339	0.3902	0.3736	0.4288	0.4505	0.4176
35	0.6220	0.8850	0.7439	0.5695	0.8131	0.6613	0.6813
36	0.5202	0.7768	0.9695	0.5103	0.6914	0.9425	0.7147
37	1.0000	0.8218	0.0000	1.0000	0.7373	0.3333	0.6902
38	0.1273	0.0000	0.4572	0.3642	0.3333	0.4795	0.3924
39	0.8283	0.7048	0.5060	0.7444	0.6288	0.5030	0.6254
40	0.5783	0.4412	0.4329	0.5425	0.4722	0.4685	0.4944
41	0.5589	0.5698	0.2377	0.5313	0.5375	0.3961	0.4883
42	0.3453	0.7080	0.4572	0.4330	0.6313	0.4795	0.5146
43	0.1026	0.2220	0.2377	0.3578	0.3913	0.3961	0.3817
44	0.4086	0.2382	0.4329	0.4581	0.3963	0.4685	0.4410
45	0.4456	0.3216	0.5182	0.4742	0.4243	0.5093	0.4693
46	0.5391	0.6407	0.2499	0.5203	0.5819	0.4000	0.5007

Table 4 ANOVA table of GRG

Source	Sum of squares	df	Mean square	*F*-value	*p*-value
Model	0.4797	20	0.0240	7.43	< 0.0001
I	0.0766	1	0.0766	23.74	< 0.0001
V	0.1395	1	0.1395	43.23	< 0.0001
T_{ON}	0.0640	1	0.0640	19.84	0.0002
T_{OFF}	0.0007	1	0.0007	0.2053	0.6544
DP	0.0061	1	0.0061	1.89	0.1815
I × V	0.0120	1	0.0120	3.71	0.0656
I × T_{ON}	0.0070	1	0.0070	2.16	0.1537
I × T_{OFF}	0.0049	1	0.0049	1.53	0.2274
I × DP	0.0002	1	0.0002	0.0525	0.8206
V × T_{ON}	0.0505	1	0.0505	15.65	0.0006
V × T_{OFF}	0.0007	1	0.0007	0.2187	0.6441
V × DP	0.0020	1	0.0020	0.6317	0.4342
T_{ON} × T_{OFF}	0.0015	1	0.0015	0.4654	0.5014
T_{ON} × DP	0.0004	1	0.0004	0.1143	0.7381
T_{OFF} × DP	0.0013	1	0.0013	0.3999	0.5329
I^2	0.0004	1	0.0004	0.1283	0.7232
V^2	0.0507	1	0.0507	15.72	0.0005
T_{ON}^2	0.0288	1	0.0288	8.93	0.0062
T_{OFF}^2	0.0025	1	0.0025	0.7892	0.3828
DP^2	0.0000	1	0.0000	0.0036	0.9525
Residual	0.0807	25	0.0032		
Lack of fit	0.0550	20	0.0028	0.5356	0.8545
Pure error	0.0257	5	0.0051		
Cor. total	0.5604	45			

$$\begin{aligned} GRG = \quad & 1.23663 - 0.04049I + 0.014423V - 0.30813T_{ON} + 0.13588T_{OFF} \\ & -0.00318DP + 0.001094I\ V - 0.00418I\ T_{ON} - 0.00352I\ T_{OFF} \\ & +0.000052I\ DP + 0.005618V\ T_{ON} + 0.000664V\ T_{OFF} + 0.00009V\ DP \\ & -0.00484T_{ON}\ T_{OFF} + 0.00019T_{ON}DP - 0.00036T_{OFF}DP + 0.000276I^2 \\ & -0.00076V^2 + 0.014368T_{ON}^2 - 0.00427_{OFF}^2 + 0.00000185DP^2 \end{aligned} \tag{8}$$

The next step of analysing the result as the mathematical multi-regression model was to optimize the process. The GRG model is a unified model that requires maximizing. Therefore, the genetic algorithm (GA) was employed for the tri-objective optimization through GRA. GA is a population-based method of optimization inspired by nature [60, 61]. The first step defined the population size (P_S), crossover (P_{CO}) and mutation (P_{MU}) probabilities and crossover (I_{CO}) and mutation (I_{MU}) indices. The number of iterations required to evaluate the unified function (GRG) was required as the termination criteria. On the contrary, the termination was taken within the iteration number where all the population members carry the same value. Each iteration consists of a selection of a mating pool, crossover to generate an equal number of offspring, mutation of the offspring and, at last, the survival of the fittest.

The binary tournament selection was considered for getting the mating pool. Each member of the population should have to go through the tournament selection process twice, and one member should be selected based on the relative fitness values.

In this step, the member with the best fitness was selected twice for the mating pool. The next step was the crossover, and simulated binary crossover (SBX) was selected. Based on the value of random numbers, the crossover is either to be there or the parents considered as offspring.

In this SBX crossover, two members from the mating pool were selected randomly. Then, based on another random number (R), the crossover was decided with respect to the probability of crossover (P_{CO}) [62, 63]. If $R \geq P_{CO}$, the crossover is not required, and the parents were moved further as the two offspring. Otherwise, a crossover is required to have the two offspring. Hence, a pool (U) of n random numbers was selected that depends on variable counts (n) considered for the problem and shown as Eq. 9. Finally, the pool of random numbers was used to calculate the β_{in} values for each variable for the crossover using Eq. 10. Then, two offspring are generated using Eq. 11 and corner-bounding the offspring to bring them inside the solution space. Corner-bounding is required either for the variable higher than its upper bound or lower than its lower bound.

$$U = [U_1 U_2 U_3 \ldots\ldots\ldots U_n] \tag{9}$$

$$\beta = \begin{cases} (2U_{in})^2, & if\ U_{in} \leq 0.05 \\ \left(\frac{1}{2(1-U_{in})}\right)^{1/(I_{co}+1)}, & otherwise \end{cases} \tag{10}$$

$$O_{i,in} = \begin{cases} 0.5[(1+\beta_{in})P_i + (1-\beta_{in})P_{i+1}],\ where\ i = 1\ and\ in = 1, 2, 3, \ldots.n \\ 0.5[(1+\beta_{in})P_i + (1-\beta_{in})P_{i-1}],\ where\ i = 2\ and\ in = 1, 2, 3, \ldots.n \end{cases} \tag{11}$$

After each member of the mating pool crossover, the polynomial mutation was considered as per the mutation probability (P_{MU}) and index of mutation (I_{MU}). Then, each offspring was checked for the possibility of mutation depending on P_{MU} and a random number [64, 65]. No offspring mutation existed if the random number was more than the P_{MU}. Otherwise, the mutation happens to the offspring. The mutation requires a pool of random numbers (r) equal to the number of variables considered, as shown in Eq. 12. The δ_{in} was calculated as per the value of the r_i using Eq. 13 and then the mutated offspring (O_m) using Eq. 14 through the use of the uber bound (UB) and the lower bound (LB) of each variable.

$$r = [r_1 r_2 r_3 \ldots\ldots\ldots r_n] \tag{12}$$

$$\delta_{in} = \begin{cases} (2ri)^{1/(I_{MU}+1)} - 1, & if\ r_i < 0.05 \\ 1 - [2(1-ri)]^{1/(I_{MU}+1)}, & otherwise \end{cases} \tag{13}$$

$$O_{m,j} = O_{o,in} + (UB_{in} - LB_{in})\delta_{in} \tag{14}$$

Then, all the parents and offspring were considered together for the natural selection of survival of the fittest. The best P_S members were selected from the $2P_S$ solutions depending on their fitness values in the next iteration. The optimized process

control parameters were found when all the P_S members had the same fitness values and each member's variables were the same.

Results and discussion

As this article deals with a hybrid optimisation approach, i.e. GA assisted by GRA, the various behaviours of GRG are discussed first. Therefore, Fig. 5 shows the interaction plots for GRG's truly influential process parameters found using ANOVA, shown in Table 2. The interaction plot concerns the influences of discharge current (I), servo voltage (V) and the rest of the process parameters at constant values found through GA's optimisation process.

The other process parameters are the discharge time of the spark (T_{ON}), the charging time of the capacitor blanks (T_{OFF}) and dielectric pressure (DP) at 2 µs, 9 µs and 50 kg/cm^2, respectively. The graph shows that the GRG falls by raising the servo gap voltage (V) and vice versa. It also shows that at V of 40 V and I of 12 A, the predicted GRG was 0.9888, whereas it was at 0.7413 at $V=40$ V and $I=22$ A. Hence, the GRG also falls by raising the discharge current. At higher servo gap voltage, the GRG falls concerning the rise of the discharge current, but its fall is lower than low servo gap voltage.

Figure 6 shows the predicted and actual values variation of GRG. The graph shows a maximum of 14.87% more prediction of GRG than the actual GRG at experimental set 41. Conversely, at experimental set 37, a maximum of 18.73% less prediction of GRG than the actual. There is an average of 0.55% more prediction of GRG than the actual one.

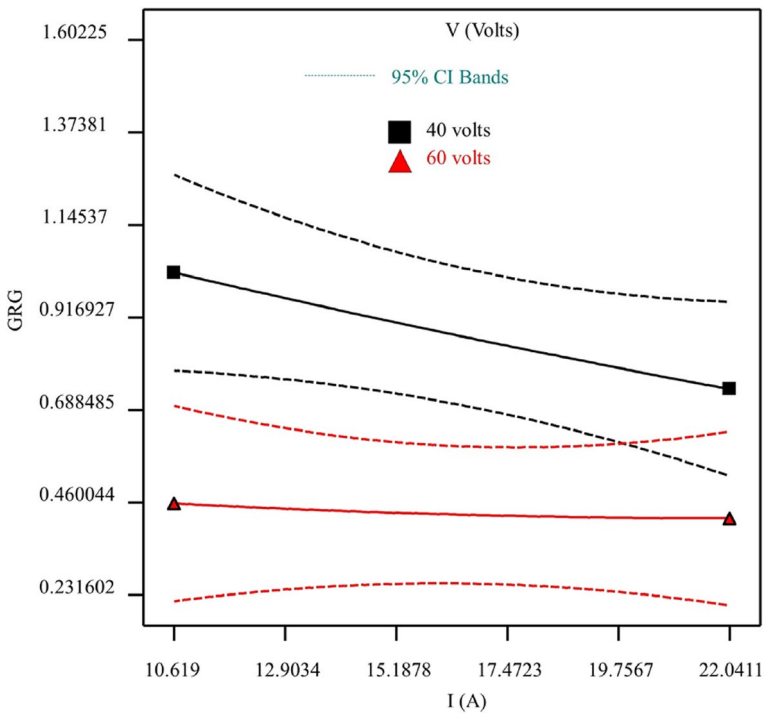

Fig. 5 Interaction plots for GRG concerning its most influential process parameters

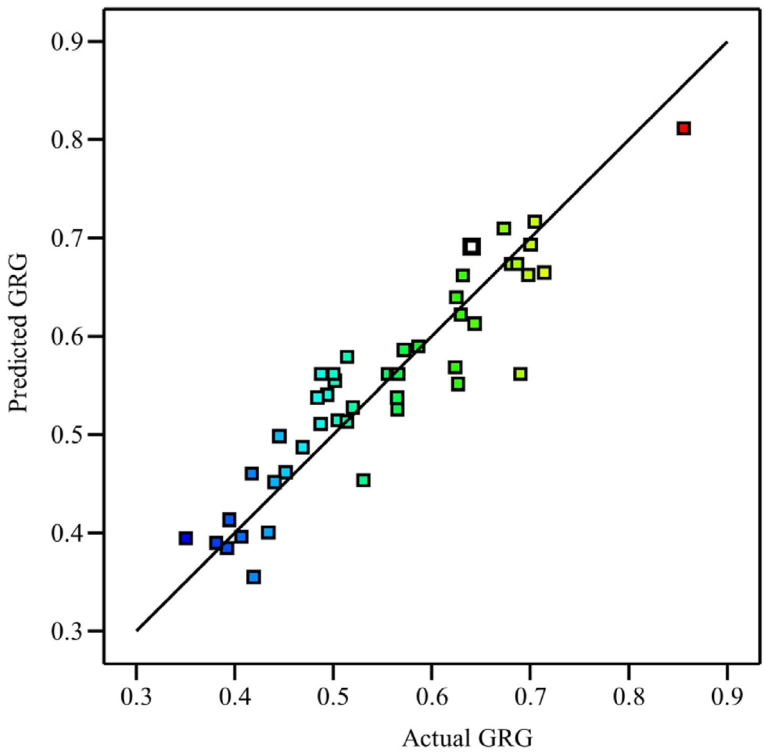

Fig. 6 Predicted versus actual GRG

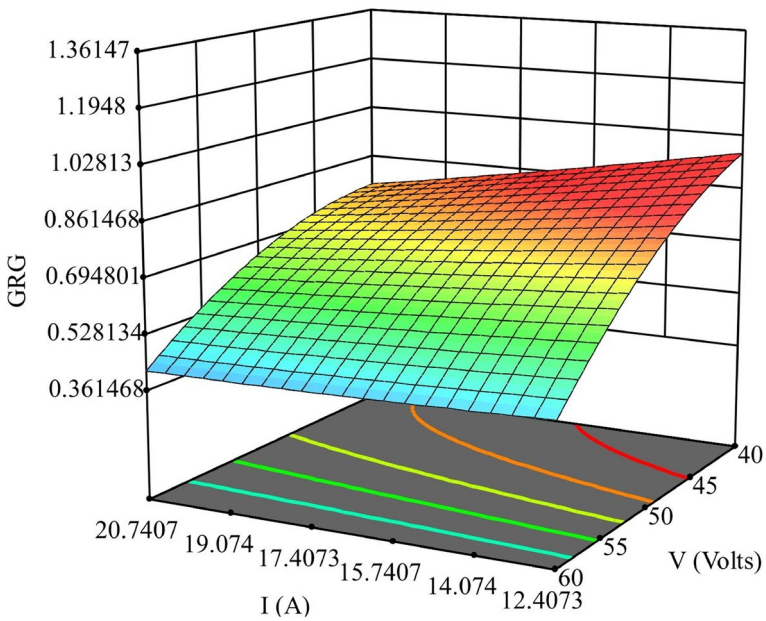

Fig. 7 Surface and contour plots for GRG concerning I and V

As discussed earlier, Fig. 7 displays the surface chart for the GRG concerning I and V at the optimum set. It is clear from the graphs that at lower servo gap voltage, the GRG is highest at lower discharge current. Whereas at an enormous servo voltage,

the GRG is minimal. The variation of GRG is low due to the variation in discharge current at a superior servo voltage.

Figure 8 indicates the variation MRR as the surface plot involving the GRG's most influencing process parameters. The graphs show that at higher servo gap voltage and lower discharge current, the MRR is not possible due to insufficient energy available for the material removal. By raising discharge current (I) and lowering the servo voltage, the MRR moves to its higher value, about 0.00904 g/min, whereas at about 21.98 A and 42.06 V, the MRR is at its maximum predicted, 0.0091 g/min. The MRR rises with the discharge current [66]. The higher MRR required is due to the maximum possible energy utilization for the melting and evaporating of the work material.

Figures 9 and 10 show the surface plots concerning TWR and DoT, the lower, the better responses, respectively, at the optimum control parameters with the variation of the most substantial process parameters I and V. The TWR graphs show that its required lower value is around 0.0044 g/min at about 12.11 A of discharge current and 42.001 V of servo gap voltage. This lower TWR is because the energy the electrode receives from the spark dissipates more promptly through conduction into the electrode and convention into the flushed distilled water, the dielectric fluid. On the contrary, the unwanted rise of TWR is predicted at elevated servo voltage and discharge current and reaches approximately 0.0322 g/min [67]. The DoT graphs also show the same trend type as the TWR.

Figure 10 shows the favourable DoT value, i.e. 0 radians bounded by the area between 12 A and 54 V and 22 A and 42 V. The minimum DoT value of 0 radians means that the tool wear raises the work-electrode gap at the hole's top surface, reducing excessive sparking at the top side of the hole. It led to shelf adjustment of the hole to a predicted perfect right cylindrical hole. In contrast to a perfect predicted

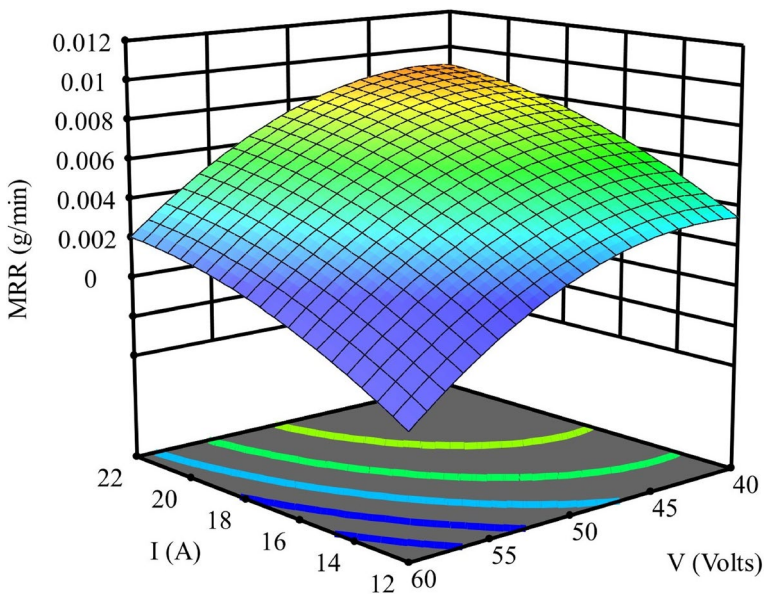

Fig. 8 Surface plot for MRR concerning I and V

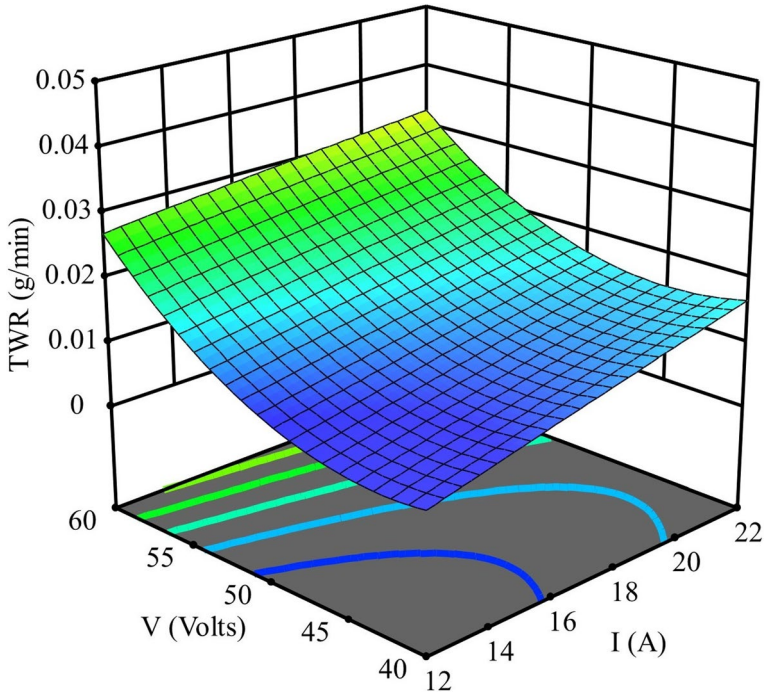

Fig. 9 Surface plot for TWR concerning I and V

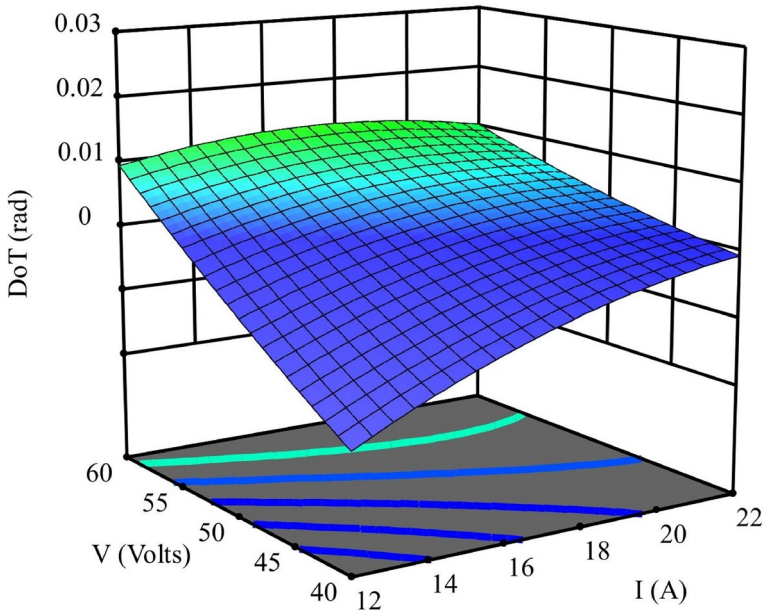

Fig. 10 Surface plot for DoT concerning I and V

hole, the unwanted DoT value reaches a maximum of about 0.0128 radians, approximately at 18 A of discharge current and 60 V of servo gap voltage [68].

The genetic algorithm (GA) optimized the GRG quadratic equation through MATLAB programming. The population was considered to have 20 members, four times

the counts of process parameters. The termination criteria for the GA was 20 iterations, and the optimum conditions were reached for each condition within 20 generations. Another set of GA parameters is the crossover (I_{CO}) and mutation (I_{MU}) indices, 20 each; as the values of the indices are higher, the offspring generated closer to their parents. Finally, the crossover (P_{CO}) and mutations (P_{MU}) probabilities were decided through the algorithm, considering that the P_{CO} should be higher and the P_{MU} should be lower. At $P_{CO} = 0.5$ and $P_{MU} = 0.4$, the optimum setting after which the results are the same, i.e. all combinations of P_{CO} greater than 0.5 and P_{MU}, varies between 0.1 and 0.5. All the above parametric settings of GA lead to the optimum control process parameters as I of 12 A, V of 40 V, T_{ON} of 2 µs, T_{OFF} of 9 µs and DP of 50 kg/cm^2.

The assenting experiment checked the boldness of the optimum setting concerning the predicted responses, as provided in Table 5. It can be realized from the table that percentage of variation of the predicted values of the responses with respect to the experimental values; MRR predicts 2.78% less than its experimental value, and the TWR and DoT were predicted at 26.32% and 35.96%, respectively, more than their experimental values. The higher deviations of the TWR and DoT are due to measurement errors. The weight, diameter and time errors are 0.001 g, 0.01 mm and 0.001 s, respectively. These errors are tiny, but the overall weight of the electrode is relatively low, and the diameters of the drilled holes on both sides are low. Therefore, it leads to much higher deviations in the TWR and DoT.

Figure 11 shows the SEM image of the top side of the EDM drilled hole for the optimum parametric setting. More material was removed adjacent to the EDM drilled hole due to the spark's erratic behaviour. Recast layers are visible in the vicinity, and cracks on them imply a higher rate of cooling of the molten material on the surface of the workpiece. Micro pits are also visible on the drilled hole surface, indicating the impact of the spark. A few macro pits were formed around the micro EDM drilled hole.

Conclusions

The shape memory behaviour of Nitinol can be altered during thermal processing. Therefore, thermal processing needs optimization. Hence, this experimental work on micro-EDM drilling operation has been carried out by selecting process parameters such as discharge current (I), discharge time (T_{ON}), charging time (T_{OFF}), servo gap voltage (V) and dielectric flushing pressure (DP). The experiment was designed using a Box-Behnken design, and the material removal rate (MRR), tool wear rate (TWR), and degree of hole taper (DoT) were considered as the responses. The tri-response optimization was carried through grey relational grade (GRG)-assisted genetic algorithm (GA) of

Table 5 Experimental, predicted and percentage of variations of responses at the optimized process control parametric setting

Responses	Units	Experimental value	Predicted value	% variation
MRR	g/min	0.0036	0.0035	− 2.78
TWR	g/min	0.0038	0.0048	26.32
DoT	rad	0.0089	0.0121	35.96

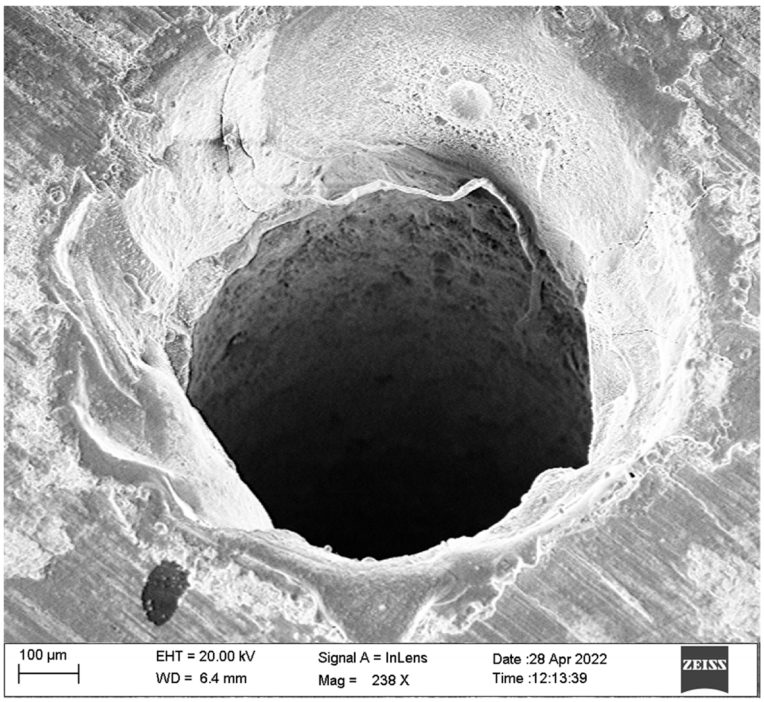

Fig. 11 SEM image of the micro EDM drilled hole

µ-EDM drilling on $Ni_{51.58}Ti_{48.34}$ alloy using a copper tubular electrode and demineralized water (dielectric fluid). The following conclusions are drawn:

i. The tri-regression analysis using the quadratic GRG model provides the mathematical model's significance through variance analysis; the spark's discharge current (I) and the servo voltage (V) were the most substantial process parameters.
ii. The GRA-assisted GA offers the optimum parametric set I of 12 A, V of 40 V, T_{ON} of 2 µs, T_{OFF} of 9 µs and DP of 50 kg/cm^2.
iii. The confirmatory experiment at the optimized control parametric setting provides the experimental MRR, TWR and DoT, and their predicted values vary by 2.78, 26.32 and 35.96%, respectively.

The future directions of the research work might include surface quality, hole circularity and heat-affected zones for micro-EDM drilling of the Nitinol, shape memory alloy and the optimization of the responses through other techniques.

Abbreviations

MRR (g/min)	Material removal rate
TWR (g/min)	Tool wear rate
DoT (radians)	Degree of hole taper
BBD	Box-Behnken design
DOE	Design of experiment
GRA	Grey relational analysis
GRG	Grey relational grades
GA	Genetic algorithm
X_{Ni}	Normalized ith response
X_{in}	Ith response
X_{max}	Maximum value of the responses

X_{min}	Minimum value of the responses
GRC	Grey relational coefficient
ΔX_{min}	Minimum value of deviation sequence
ΔX_{max}	Maximum value of deviation sequence
ANOVA	Analysis of variance
I (Amp)	Discharge current
V (volts)	Servo voltage
T_{ON} (μs)	Discharge time
T_{OFF} (μs)	Charging time
DP (kg/cm^2)	Dielectric flushing pressure
P_S	Population size
P_{CO}	Crossover probability
P_{MU}	Mutation probability
I_{CO}	Index of crossover
I_{MU}	Index of mutation
SBX	Simulated binary crossover
R	A random numbers
U, r	Pools of random numbers
n	Number of variables
β_{in}, δ_{in}	Constants
U_{in}, r_i	I^{th} random number of the pools
$O_{i,in}$, O_m	I^{th} offspring and mutated offspring
P_i, P_{i+1}	I^{th} and $(i+1)^{th}$ parent

Acknowledgements
We are glad to acknowledge the help of Mr. Bhanu Pratap Arya, the lab staff, the Mechanical Engineering Department, JUET, and Guna during the experimental work.

Authors' contributions
AKS contributed with preparation of DOE, experimentation, theoretical analysis of the experimental result, conduction of the different testing and validation experiments based on the experimental results. DRM contributed with problem formulation, verification of the confirmation experimental results of the article and review of the manuscript. All authors have read and approved the final manuscript.

Funding
The authors did not receive funding from any organization for the experimental work.

Availability of data and materials
The datasets used and/or analysed during the current study are available from the corresponding author on reasonable request.

Declarations

Competing interests
The authors declare that they have no competing interests.

Received: 25 February 2024 Accepted: 1 May 2024
Published online: 15 May 2024

References

1. Duerig T, Pelton A, Stö D, Stöckel D (1999) An overview of nitinol medical applications. Mater Sci Eng, A 273–275:149–160. https://doi.org/10.1016/S0921-5093(99)00294-4
2. Welsch G, Boyer R, Collings EW (1998) Materials properties handbook: titanium alloys, 2nd edn.
3. Guo Y, Klink A, Fu C, Snyder J (2013) Machinability and surface integrity of nitinol shape memory alloy. CIRP Ann 62:83–86. https://doi.org/10.1016/j.cirp.2013.03.004
4. Dash B, Das M, Das M, Mahapatra TR, Mishra D (2019) A concise review on machinability of NiTi shape memory alloys
5. Malhotra P, Singh NK, Tyagi RK, Sikarwar BS (2021) Comparative study of rotary-EDM, gas assisted-EDM, and gas assisted powder mixed-EDM of the hybrid metal matrix composite. Adv Mater Proc Technol 7:27–41. https://doi.org/10.1080/2374068X.2020.1855398
6. Plaza S, Sanchez JA, Perez E, Gil R, Izquierdo B, Ortega N, Pombo I (2014) Experimental study on micro EDM-drilling of Ti6Al4V using helical electrode. Precis Eng 38:821–827. https://doi.org/10.1016/j.precisioneng.2014.04.010
7. Tanjilul M, Ahmed A, Kumar AS, Rahman M (2018) A study on EDM debris particle size and flushing mechanism for efficient debris removal in EDM-drilling of Inconel 718. J Mater Process Technol 255:263–274. https://doi.org/10.1016/j.jmatprotec.2017.12.016
8. Khan F, kumar J, Soota T (2019) Optimization of EDM process parameter for stainless steel D3. Mater Today Proc 7–10. https://doi.org/10.1016/j.matpr.2019.07.529

9. Tiwari V, Mishra DR (2016) Multi response optimization of EDM paramerers for Monel K-500. Int J Adv Prod Mech Eng 2:53–60
10. Chakala N, Chandrabose PS, Rao CSP (2021) Optimisation of WEDM parameters on nitinol alloy using RSM and desirability approach. Aust J Mech Eng 19:582–594. https://doi.org/10.1080/14484846.2019.1681239
11. Kim J, Park J-K, Kim HK, Unnithan AR, Kim CS, Park CH (2017) Optimization of electropolishing on NiTi alloy stents and its influence on corrosion behavior. J Nanosci Nanotechnol 17:2333–2339. https://doi.org/10.1166/jnn.2017.13324
12. Lee J, Shin YC (2019) Effects of composition and post heat treatment on shape memory characteristics and mechanical properties for laser direct deposited nitinol. Lasers Manufac Mater Proc 6:41–58. https://doi.org/10.1007/s40516-019-0079-5
13. Li S, Cui Z, Zhang W, Li Y, Li L, Gong D (2019) Biocompatibility of micro/nanostructures nitinol surface via nanosecond laser circularly scanning. Mater Lett 255:126591. https://doi.org/10.1016/j.matlet.2019.126591
14. Chaudhari R, Vora JJ, Patel V, López de Lacalle LN, Parikh DM (2020) Surface analysis of wire-electrical-discharge-machining-processed shape-memory alloys. Materials 13:530. https://doi.org/10.3390/ma13030530
15. Lojen G, Stambolić A, Šetina Batič B, Rudolf R (2020) Experimental continuous casting of nitinol. Metals (Basel) 10:505. https://doi.org/10.3390/met10040505
16. Datta S, Raza MS, Das AK, Saha P, Pratihar DK (2020) Experimental investigations and parametric optimization of laser beam welding of nitinol sheets by metaheuristic techniques and desirability function analysis. Opt Laser Technol 124:105982. https://doi.org/10.1016/j.optlastec.2019.105982
17. Ikeuchi Y, Fujii K, Okada A (2020) Fundamental investigation on EDM characteristics of lanthanum hexaboride applied for cathode parts. Int J Elec Mach 25:27. https://doi.org/10.2526/ijem.25.27
18. Ming W, Shen F, Zhang Z, Huang H, Du J, Wu J (2020) A comparative investigation on magnetic field–assisted EDM of magnetic and non-magnetic materials. Int J Adv Manuf Technol 109:1103–1116. https://doi.org/10.1007/s00170-020-05653-8
19. Ilani MA, Khoshnevisan M (2020) Powder mixed-electrical discharge machining (EDM) with the electrode is made by fused deposition modeling (FDM) at Ti-6Al-4V machining procedure. Multiscale and Multidisciplinary Modeling, Experiments and Design 3:173–186. https://doi.org/10.1007/s41939-020-00070-6
20. Paswan K, Pramanik A, Chattopadhyaya S, Basak AK (2020) A novel approach towards sustainable electrical discharge machining of metal matrix composites (MMCs). Int J Adv Manuf Technol 106:1477–1486. https://doi.org/10.1007/s00170-019-04816-6
21. Baran A, Polanski M (2018) Microstructure and properties of LENS (laser engineered net shaping) manufactured Ni-Ti shape memory alloy. J Alloys Compd 750:863–870. https://doi.org/10.1016/j.jallcom.2018.03.400
22. Pelton AR, Dicello J, Miyazaki S (2000) Optimisation of processing and properties of medical grade nitinol wire. Minim Invasive Ther Allied Technol 9:107–118. https://doi.org/10.3109/13645700009063057
23. Roy BK, Mandal A (2019) Surface integrity analysis of nitinol-60 shape memory alloy in WEDM. Mater Manuf Processes 34:1091–1102. https://doi.org/10.1080/10426914.2019.1628256
24. Lee ES, Shin TH (2011) An evaluation of the machinability of nitinol shape memory alloy by electrochemical polishing. J Mech Sci Technol 25:963–969. https://doi.org/10.1007/s12206-011-0209-2
25. Kowalczyk M, Nižankowski C (2017) Comparative analysis of machinability of nitinol alloy using weighted radar diagram. Manage Prod Eng Rev 8:74–81. https://doi.org/10.1515/mper-2017-0038
26. Shiek J, Sairam J, Mouda PA (2023) Parameter optimization in the enhancement of MRR of titanium alloy using newer mixing method in PMEDM process. J Eng Appl Sci 70:59. https://doi.org/10.1186/s44147-023-00230-8
27. Sharma P, Singh S, Mishra DR (2014) Electrical discharge machining of AISI 329 stainless steel using copper and brass rotary tubular electrode. Proc Mater Sci 5:1771–1780. https://doi.org/10.1016/j.mspro.2014.07.367
28. Quarto M, D'Urso G, Giardini C (2022) Micro-EDM optimization through particle swarm algorithm and artificial neural network. Precis Eng 73:63–70. https://doi.org/10.1016/j.precisioneng.2021.08.018
29. Abhilash PM, Chakradhar D (2022) Multi-response optimization of wire EDM of Inconel 718 using a hybrid entropy weighted GRA-TOPSIS method. Proc Integr Optimization Sustain 6:61–72. https://doi.org/10.1007/s41660-021-00202-6
30. Naik R, Sathisha N (2022) Desirability function and GA-PSO based optimization of electrochemical discharge micro-machining performances during micro-channeling on silicon-wafer using mixed electrolyte. SILICON. https://doi.org/10.1007/s12633-022-01697-5
31. Sree Ram H, Uthayakumar M, Suresh Kumar S, Thirumalai Kumaran S, Azzopardi B, Korniejenko K (2022) Prediction of kerf width and surface roughness of Al6351 based composite in wire-cut electric discharge machining using mathematical modelling. Materials 15:1102. https://doi.org/10.3390/ma15031102
32. Pandey S, Shrivastava PK, Dangi S, Singh P (2022) Experimental modelling and optimisation of electrical arc machining of Al-B4C metal matrix composite. Aust J Mech Eng 20:245–255. https://doi.org/10.1080/14484846.2019.1701395
33. Sisodiya MS, Shukla S, Bajpai V (2022) Feasibility analysis of novel Maglev EDM by comparing with conventional micro EDM. Sci Rep 12:2613. https://doi.org/10.1038/s41598-022-06662-1
34. Kiran P, Mohanty S, Das AK (2022) Surface modification through sustainable micro-EDM process using powder mixed bio-dielectrics. Mater Manuf Processes 37:640–651. https://doi.org/10.1080/10426914.2021.1967976
35. Baroi BK, Jagadish PPK (2022) A review on sustainability, health, and safety issues of electrical discharge machining. J Braz Soc Mech Sci Eng 44:59. https://doi.org/10.1007/s40430-021-03351-4
36. Ablyaz TR, Shlykov ES, Muratov KR, Zhurin AV (2022) Study of the EDM process of bimetallic materials using a composite electrode tool. Materials 15. https://doi.org/10.3390/ma15030750
37. Rajaguru J, Kumar P, Arunachalam N (2022) Novel carbon nanotubes reinforced copper composite electrode for improved performance of electric discharge machining. Mater Lett 307:131063. https://doi.org/10.1016/j.matlet.2021.131063

38. Kumar H, Davim JP (2011) Role of powder in the machining of Al-10%Sic $_p$ metal matrix composites by powder mixed electric discharge machining. J Compos Mater 45:133–151. https://doi.org/10.1177/0021998310371543
39. Fasina E, Sawyerr BA, Abdullahi YU, Oke SA (2023) A comparison of two hybrid optimization techniques: the Taguchi-BBD-firefly and the Taguchi-regression-firefly methods on the IS 2062–E250 steel plates boring problem. J Eng Appl Sci 70:47. https://doi.org/10.1186/s44147-023-00215-7
40. Muralidharan B, Prabu K, Rajamurugan G (2021) Pulsed Nd:YAG laser machining of nitinol: an experimental investigation. Journal of Micromanufacturing 251659842110154. https://doi.org/10.1177/25165984211015482
41. Hung JC, Yang PJ (2021) Electrochemical microslot machining by ultrasonic-vibration-aided electrolyte on nitinol wire. Processes 9. https://doi.org/10.3390/pr9101752
42. Kumar Sahu A, Chatterjee S, Kumar Nayak P, Mahapatra SS (2018) Study on effect of tool electrodes on surface finish during electrical discharge machining of nitinol. In: IOP Conference Series: Materials Science and Engineering
43. Kulkarni VN, Gaitonde VN, Aiholi V, Hadimani V (2018) Multi performance characteristics optimization in wire electric discharge machining of nitinol superelastic alloy. Mater Today Proc 5:18857–18866. https://doi.org/10.1016/j.matpr.2018.06.233
44. Pradhan S, Dash PB, Kumari K, Dhupal D (2021) Study of micro machining characteristics by Nd-YAG Laser on nitinol shape memory alloy. Adv Mater Proc Technol 1–15. https://doi.org/10.1080/2374068X.2021.1946757
45. Liu JF, Guo YB, Butler TM, Weaver ML (2016) Crystallography, compositions, and properties of white layer by wire electrical discharge machining of nitinol shape memory alloy. Mater Des 109:1–9. https://doi.org/10.1016/j.matdes.2016.07.063
46. Duerig TW, Pelton AR, Bhattacharya K (2017) The measurement and interpretation of transformation temperatures in nitinol. Shape Memory Superelasticity 3:485–498. https://doi.org/10.1007/s40830-017-0133-0
47. Sahoo AK, Pandey P, Mishra DR (2021) Multi-response optimization of EDM drilling parameters of the nitinol SMA. J Eng Exact Sci 7. https://doi.org/10.18540/jcecvl7iss4pp13007-01-17e
48. Kılıç B (2019) Determination of wind dissipation maps and wind energy potential in Burdur province of Turkey using geographic information system (GIS). Sustainable Energy Technologies and Assessments 36. https://doi.org/10.1016/j.seta.2019.100555
49. Mishra DR, Bajaj A, Bisht R (2020) Optimization of multiple kerf quality characteristics for cutting operation on carbon–basalt–Kevlar29 hybrid composite material using pulsed Nd:YAG laser using GRA. CIRP J Manuf Sci Technol 30:174–183. https://doi.org/10.1016/j.cirpj.2020.05.005
50. Taşkan E, Bulak S, Taşkan B, Şaşmaz M, el Abed S, el Abed A (2019) Nitinol as a suitable anode material for electricity generation in microbial fuel cells. Bioelectrochemistry 128:118–125. https://doi.org/10.1016/j.bioelechem.2019.03.008
51. Guo Y, Klink A, Fu C, Snyder J (2013) Machinability and surface integrity of nitinol shape memory alloy. CIRP Ann Manuf Technol 62:83–86. https://doi.org/10.1016/j.cirp.2013.03.004
52. Mishra DR, Gautam GD, Prakash D, Bajaj A, Sharma A, Bisht R, Gupta S (2020) Optimization of kerf deviations in pulsed nd: YAG laser cutting of hybrid composite laminate using GRA. FME Transactions 48:109–116. https://doi.org/10.5937/fmet2001109M
53. Paszkowicz W (2013) Genetic algorithms, a nature-inspired tool: a survey of applications in materials science and related fields: part II. Mater Manuf Processes 28:708–725. https://doi.org/10.1080/10426914.2012.746707
54. MsT B, MrOK K, MrNK K, MsSL P, Kakandikar GM, Nandedkar VM (2015) Genetic algorithm and its applications to mechanical engineering: a review. Mater Today Proc 2:2624–2630. https://doi.org/10.1016/j.matpr.2015.07.219
55. Reddy VC, Gowd GH, Kumar MLSD (2018) Empirical modeling & optimization of laser micro - machining process parameters using genetic algorithm. In: Materials Today: Proceedings
56. Kilickap E, Huseyinoglu M, Yardimeden A (2011) Optimization of drilling parameters on surface roughness in drilling of AISI 1045 using response surface methodology and genetic algorithm. Int J Adv Manuf Technol 52:79–88. https://doi.org/10.1007/s00170-010-2710-7
57. Gautam G, Mishra D (2019) Evaluation of geometrical quality characteristics in pulsed Nd:YAG laser cutting of Kevlar-29/basalt fiber reinforced hybrid composite using grey relational analysis based on genetic algorithm. FME Transactions 47:560–575. https://doi.org/10.5937/fmet1903560G
58. Guo J, Wang B, He ZX, Pan B, Du DX, Huang W, Kang RK (2021) A novel method for workpiece deformation prediction by amending initial residual stress based on SVR-GA. Adv Manuf 9:483–495. https://doi.org/10.1007/s40436-021-00368-9
59. Davim JP (2015) Design of experiments in production engineering
60. Rao SS (2009) Engineering optimization. John Wiley & Sons Inc, Hoboken
61. Sampreet KR, Mahidhar V, Narayanan RK, Kannan TDB (2021) Optimization of process parameters in laser welding of Hastelloy C-276 using artificial neural network and genetic algorithm. Surf Rev Lett 28:2050042. https://doi.org/10.1142/S0218625X20500420
62. Saravanakumar, Valarmathi K, Pallikonda Rajasekaran M, Srinivasan S, Willjuice Iruthayarajan M, Balas VE (2015) Tuning of multivariable decentralized PID controller using state transition algorithm. Studies Inform Control 24. https://doi.org/10.24846/v24i4y201501
63. Pan L, Xu W, Li L, He C, Cheng R (2021) Adaptive simulated binary crossover for rotated multi-objective optimization. Swarm Evol Comput 60. https://doi.org/10.1016/j.swevo.2020.100759
64. Zeng GQ, Chen J, Li LM, Chen MR, Wu L, Dai YX, Zheng CW (2016) An improved multi-objective population-based extremal optimization algorithm with polynomial mutation. Inf Sci (N Y) 330. https://doi.org/10.1016/j.ins.2015.10.010
65. Alawad NA, Abed-alguni BH (2021) Discrete Island-Based Cuckoo Search with highly disruptive polynomial mutation and opposition-based learning strategy for scheduling of workflow applications in cloud environments. Arab J Sci Eng 46. https://doi.org/10.1007/s13369-020-05141-x

66. Kanagarajan D, Karthikeyan R, Palanikumar K, Davim JP (2008) Optimization of electrical discharge machining characteristics of WC/Co composites using non-dominated sorting genetic algorithm (NSGA-II). Int J Adv Manuf Technol 36:1124–1132. https://doi.org/10.1007/s00170-006-0921-8
67. Magabe R, Sharma N, Gupta K, Paulo Davim J (2019) Modeling and optimization of Wire-EDM parameters for machining of Ni55.8Ti shape memory alloy using hybrid approach of Taguchi and NSGA-II. Int J Adv Manuf Technol 102:1703–1717. https://doi.org/10.1007/s00170-019-03287-z
68. Davim JP (2013) Nontraditional machining processes: research advances

Publisher's Note